

PAPER • OPEN ACCESS

Origin of the anomalous electromechanical interaction between a moving magnetic dipole and a closed superconducting loop

To cite this article: Hongye Zhang *et al* 2022 *Supercond. Sci. Technol.* **35** 045009

View the [article online](#) for updates and enhancements.

You may also like

- [Origin of dc voltage in type II superconducting flux pumps: field, field rate of change, and current density dependence of resistivity](#)
J Geng, K Matsuda, L Fu *et al.*
- [Lenz's law with aluminum foil and a lengthwise slit](#)
Rob Berls and Michael J Ruiz
- [Low-noise second-order gradient SQUID current sensors overlap-coupled with input coils of different inductances](#)
Da Xu, Jinjin Li, Shijian Wang *et al.*



IOP | ebooks™

Bringing together innovative digital publishing with leading authors from the global scientific community.

Start exploring the collection—download the first chapter of every title for free.

Origin of the anomalous electromechanical interaction between a moving magnetic dipole and a closed superconducting loop

Hongye Zhang^{1,*} , Tianhui Yang² , Wenxin Li² , Ying Xin^{2,*} , Chao Li² , Matteo F Iacchetti^{1,3} , Alexander C Smith¹  and Markus Mueller⁴ 

¹ Department of Electrical and Electronic Engineering, University of Manchester, Manchester M1 3BB, United Kingdom

² School of Electrical and Information Engineering, Tianjin University, Tianjin 300072, People's Republic of China

³ Department of Energy, Politecnico di Milano, Milan 20156, Italy

⁴ School of Engineering, University of Edinburgh, Edinburgh EH9 3JL, United Kingdom

E-mail: Hongye.Zhang@manchester.ac.uk and Yingxin@tju.edu.cn

Received 14 November 2021, revised 8 February 2022

Accepted for publication 10 February 2022

Published 25 February 2022



CrossMark

Abstract

Lenz's law states that 'the current induced in a circuit due to a change in a magnetic field is directed to oppose the change in flux and to exert a mechanical force which opposes the motion'. This statement has been widely adopted to predict many effects in electromagnetism. However, multiple recent experimental measurements have shown that the interactions between a moving permanent magnet (PM) and a closed superconducting loop can disobey the fundamental statement of Lenz's law: during the entire process of a PM threading a high temperature superconducting (HTS) coil, the current induced in the HTS coil keeps the same direction, and thus the mechanical force exerted on the PM does not always oppose its movement. The seeming 'Lenz's law-violated phenomenon', namely the anomalous electromechanical interaction between a moving PM and a closed superconducting loop, can bring about numerous potential applications in the domains of superconducting magnetic energy storage, electromagnetic ejection, and flux pumps, etc. However, the cause of this anomalous phenomenon remains controversial. By representing the PM as a magnetic dipole, taking the perfect conductor approximation for the closed superconducting loop, this paper has theoretically studied the anomalous electromechanical effect with rigorous mathematical formulae derivation. The proposed analytical equations have been verified by numerical modelling and experimental measurements, which further confirms the effectiveness of the perfect conductor approximation in ease of calculation. Results have shown that both the induced electromotive force and the intrinsic properties of the conductive loop (resistance-dominant or inductance-dominant) determine together the electromechanical

* Authors to whom any correspondence should be addressed.



Original content from this work may be used under the terms of the [Creative Commons Attribution 4.0 licence](https://creativecommons.org/licenses/by/4.0/). Any further distribution of this work must maintain attribution to the author(s) and the title of the work, journal citation and DOI.

performance of the studied energy conversion system, and the nearly zero resistivity of superconductors is the dominant cause of the anomalous phenomenon. This paper has illuminated the origin of the anomalous electromechanical interaction between a moving magnetic dipole and a closed superconducting loop, provided an efficient and reliable tool to predict the electromechanical performance of the studied energy conversion system, and is believed to deepen people's understanding of the interactions between magnetic field sources and superconductors.

Keywords: Lenz's law, closed superconducting loop, moving magnetic dipole, electromotive force, energy conversion

(Some figures may appear in colour only in the online journal)

1. Introduction

Since 1834, Lenz's law has been extensively exploited to qualitatively explain or predict a variety of electromagnetic phenomena, e.g. the induced current in a conductive loop due to the change of external magnetic flux caused by a moving magnet will impart a dragging force on the moving magnet, etc. According to Lenz's law, when a magnet passes through a conductive loop, the current induced in the loop should always oppose the flux variation brought by the magnet. Additionally, the movement of the magnet should always be impeded by a mechanical force generated by the eddy current [1, 2]. In other words, when the magnet is approaching the conductive loop, it will receive a repulsive force due to the induced current; conversely, when the magnet is leaving the conductive loop, the current in the loop will change its direction and the magnet should bear an attracting force. However, recent experimental research work [3, 4] has shown that the conventional statement of Lenz's law can be violated in the case of a permanent magnet (PM) passing through a high temperature superconducting (HTS) coil. As reported in [3], during the entire process of the PM threading the HTS coil, the induced current keeps the same circulating direction and the PM always receives repulsive forces from the coil, which exhibits an anomalous electromechanical effect (a seeming 'Lenz's law-violated phenomenon').

Although a theory of hole superconductivity was proposed in [5] trying to account for the applicability of Lenz's law in superconductors, the experimental results in [3, 4] have offered direct evidence to indicate that the fundamental description of Lenz's law has become invalid for a superconducting circuit in terms of the electromechanical behaviour. The anomalous electromechanical effect can bring about a series of novel applications, e.g. determination of the characteristic parameters of superconducting coils [6], and energy conversion/storage used for regenerative braking in urban rail transit systems [7], etc. The seeming 'Lenz's law-violated phenomenon' challenges people's customary understanding of the electromechanical interactions between a magnetic source and a conductive loop; however, a rigorous theoretical explanation for this effect remains lacking. The unclear origin of the anomalous electromechanical effect has restricted its due attention and scope of application to a large extent.

Considering the PM as a magnetic dipole, approximating the closed superconducting loop as a perfect conductor with zero resistivity, explicit mathematical formulae have been derived in this paper to quantify the current induced in the superconducting loop and the mechanical force exerted on the PM. The analytical equations have been validated by the finite element method (FEM) based numerical models and experimental measurements. The proposed formulae can not only theoretically explain the cause of the anomalous electromechanical effect, but also provide an efficient and reliable analytical tool to analyze the interactions between magnetic sources and superconductors.

2. Theoretical analysis

Figure 1 presents the diagram of the energy conversion system: a cylindrical PM moving through a superconducting loop from top ($z > 0$) to bottom ($z < 0$), in the cylindrical coordinate system. It is assumed that the central axis of the PM crosses the center of the superconducting loop during its entire moving process.

Considering the spatial distribution characteristics of magnetic fields generated by a cylindrical PM, it can be equivalised as a magnetic dipole, as shown on the right of figure 1. Firstly, let us consider the mathematical model in the cartesian coordinate system $\mathbf{o}_m-x_m y_m z_m$.

Outside the magnetic field source region, the magnetic vector potential in the space, \mathbf{A} , can be written as [8]:

$$\mathbf{A}(r_m) = \frac{\mu_0}{4\pi} \frac{\mathbf{m} \times \mathbf{r}_m}{r^3} \quad (1)$$

where μ_0 is the vacuum permeability, \mathbf{r}_m represents the distance vector between the field source and the calculated point (x_m, y_m, z_m), and \mathbf{m} denotes the magnetic moment of the magnetic dipole, yielding [8]:

$$\mathbf{m} = \frac{1}{\mu_0} \mathbf{B}_r V \quad (2)$$

where \mathbf{B}_r stands for the remanence, and V refers to the volume of the PM.

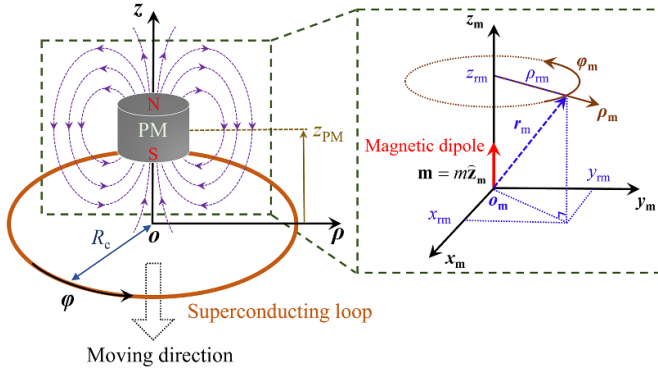


Figure 1. Diagram of a PM passing through a superconducting loop from top to bottom, in the cylindrical coordinate system $\theta-\rho\varphi z$. R_c denotes the radius of the circular loop. The PM is equivalised as a magnetic dipole, as shown on the right. To determine the spatial field distribution of the magnetic dipole, a local cartesian system $\theta_m-x_my_mz_m$ and a local cylindrical coordinate system $\theta_m-\rho_m\varphi_mz_m$ have been established.

Then, the magnetic flux density in the calculated point, \mathbf{B} , can be expressed as:

$$\mathbf{B}(r_m) = \nabla \times \mathbf{A} = \frac{\mu_0}{4\pi} \left[\frac{3\mathbf{r}_m(\mathbf{m} \cdot \mathbf{r}_m)}{r_m^5} - \frac{\mathbf{m}}{r_m^3} \right]. \quad (3)$$

The PM moves along the z_m -axis, thus \mathbf{m} can be noted as:

$$\mathbf{m} = m\hat{z}_m. \quad (4)$$

Based on (4), we have:

$$\mathbf{m} \cdot \mathbf{r}_m = mz_{rm}. \quad (5)$$

From (3)–(5), the 3D coordinate components of the magnetic field in the studied point can be derived as:

$$\begin{aligned} B_{x_m}(r_m) &= \mathbf{B} \cdot \hat{x}_m = \frac{\mu_0}{4\pi} \left[\frac{3\mathbf{r}_m(mz_{rm})}{r_m^5} - \frac{\mathbf{m}}{r_m^3} \right] \cdot \hat{x}_m \\ &= \frac{3\mu_0}{4\pi} \frac{mz_{rm}x_{rm}}{r_m^5} \end{aligned} \quad (6)$$

$$\begin{aligned} B_{y_m}(r_m) &= \mathbf{B} \cdot \hat{y}_m = \frac{\mu_0}{4\pi} \left[\frac{3\mathbf{r}_m(mz_{rm})}{r_m^5} - \frac{\mathbf{m}}{r_m^3} \right] \cdot \hat{y}_m \\ &= \frac{3\mu_0}{4\pi} \frac{mz_{rm}y_{rm}}{r_m^5} \end{aligned} \quad (7)$$

$$\begin{aligned} B_{z_m}(r_m) &= \mathbf{B} \cdot \hat{z}_m = \frac{\mu_0}{4\pi} \left[\frac{3\mathbf{r}_m(mz_{rm})}{r_m^5} - \frac{\mathbf{m}}{r_m^3} \right] \cdot \hat{z}_m \\ &= \frac{\mu_0}{4\pi} \left(\frac{3mz_{rm}^2}{r_m^5} - \frac{m}{r_m^3} \right). \end{aligned} \quad (8)$$

In order to simplify the calculation, considering the shape feature of the moving magnet and the superconducting coil, we have transformed the cartesian coordinate system to the cylindrical coordinate system, $\theta_m-\rho_m\varphi_mz_m$, as shown in figure 1.

Consequently, the spatial distribution of magnetic fields can be characterised by B_{z_m} and B_{ρ_m} ($B_{\varphi_m} = 0$), with:

$$B_{\rho_m}(r_m) = \sqrt{B_{x_m}^2 + B_{y_m}^2} = \frac{3\mu_0 m}{4\pi} \frac{\rho_m z_{rm}}{(\rho_m^2 + z_{rm}^2)^{5/2}}. \quad (9)$$

In our analytical model, the superconducting loop is fixed. Therefore, to better reflect the relative position change of the moving PM with respect to the stationary loop, let us consider the general cylindrical coordinate system for the entire model, $\theta-\rho\varphi z$, as shown in figure 1. In the coordinate system $\theta-\rho\varphi z$, $z = 0$ for the loop plane, and the varying position of the PM with respect to the loop centre is noted as z_{PM} .

The magnetic flux, Φ , through a surface of a vector area, \mathbf{S} , is defined by:

$$\Phi = \iint_S \mathbf{B} \cdot d\mathbf{S}. \quad (10)$$

Then, based on (8) and (10), the magnetic flux inside a single superconducting loop with the radius of R_c can be calculated by:

$$\begin{aligned} \Phi &= \iint_S B_z dS = \int_0^{R_c} B_z 2\pi\rho d\rho \\ &= \int_0^{R_c} \frac{\mu_0}{4\pi} \left(\frac{3mz_{PM}^2}{r^5} - \frac{m}{r^3} \right) 2\pi\rho d\rho \\ &= \frac{\mu_0 m}{2} \frac{R_c^2}{(R_c^2 + z_{PM}^2)^{3/2}} \end{aligned} \quad (11)$$

where r is the distance between the PM and the periphery of the single loop, and B_z is the transformed magnetic field along the z -axis from (8).

According to Faraday's law, the time-varying magnetic field can induce an electromotive force (EMF) on a conductive loop. Here, we underline that it should be the induced EMF (which is essentially a voltage source) and the impedance of the conductive loop that decide together the characteristics of the generated current. In a superconducting loop, the impedance is inductance-dominant because of its zero resistivity. Consequently, when a magnetic dipole threads a superconducting loop, the entire energy conversion system can be equivalised as a series circuit composed of a voltage source and an inductance, as shown in figure 2. Based on figure 2, we have:

$$-\frac{d\Phi}{dt} = L \frac{dI}{dt} \quad (12)$$

where L is the self-inductance of the superconducting loop. Equation (12) leads to constant magnetic flux, i.e. by integrating this equation, we obtain:

$$LI + \Phi = C \quad (13)$$

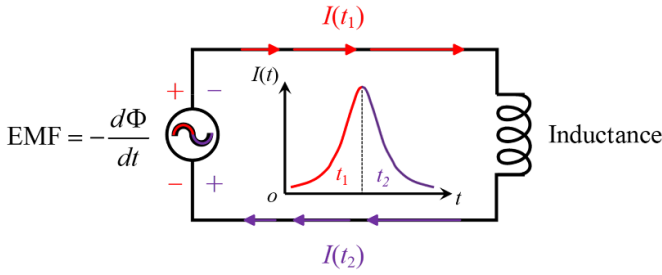


Figure 2. Equivalent electric circuit for the system of a PM threading a superconducting loop. t_1 and t_2 represent the time zones in which the PM approaches and leaves the loop, respectively.

where C refers to the flux constant. Before the movement of the PM, we suppose that it is sufficiently far from the superconducting loop and there exists no induced current, therefore $C = 0$. Then, according to (11)–(13), we have:

$$I = -\frac{\Phi}{L} = -\frac{\mu_0 m}{2L} \frac{R_c^2}{(R_c^2 + z_{PM}^2)^{3/2}} \quad (14)$$

where the negative sign demonstrates that the current circulates along the negative direction of the φ -axis.

The induced EMF is alternating and changes its sign when the PM passes through the conductive loop plane, namely the $\rho\varphi$ -plane. However, according to (14), it can be seen that the induced current does not follow the same trend as the EMF and will not change its circulating direction despite the variation of its amplitude. As a result, the current amplitude will first increase as z_{PM} varies from $+\infty$ to 0 (which happens in the time zone t_1), and then decreases when z varies from 0 to $-\infty$ (which occurs in the time zone t_2), as illustrated in figure 2. The derived equation (14) complies well with the invariance of the current direction mentioned in [3, 4].

During the entire process of the PM threading the superconducting loop, its movement is tightly affected by the mechanical force caused by the current induced in the loop. According to Newton's third law, the force imparted on the PM by the superconducting coil, \mathbf{F}_{PM} , is on the numerical level equal to the force exerted on the coil by the PM, \mathbf{F}_c , as:

$$F_{PM} = -F_c. \quad (15)$$

Therefore, to quantify the force imparted on the PM by the coil, we can directly calculate the force exerted on the coil by the PM, \mathbf{F}_c . According to Lorentz force law, we have:

$$\begin{aligned} F_c &= \int_l I \cdot (d\mathbf{l} \times \mathbf{B})_z = - \int_l I B_\rho dl = - \int_0^{2\pi} I B_\rho R_c d\varphi \\ &= -2\pi R_c I B_\rho \end{aligned} \quad (16)$$

where B_ρ is the transformed magnetic field in the radial direction from (9). It should be noted that \mathbf{B}_ρ is along the negative direction of the ρ -axis for $z > 0$ and vice versa.

On the basis of (9) and (14)–(16), F_{PM} is calculated as:

$$\begin{aligned} F_{PM} &= 2\pi R_c I B_\rho \\ &= 2\pi R_c \cdot \left[-\frac{\mu_0 m}{2L} \frac{R_c^2}{(R_c^2 + z_{PM}^2)^{3/2}} \right] \cdot \left[-\frac{3\mu_0 m}{4\pi} \frac{R_c z_{PM}}{(R_c^2 + z_{PM}^2)^{5/2}} \right] \\ &= \frac{3\mu_0^2 m^2}{4L} \frac{R_c^4 z_{PM}}{(R_c^2 + z_{PM}^2)^4}. \end{aligned} \quad (17)$$

It can be seen from (17) that the direction of the mechanical force experienced by the PM is determined by z_{PM} , and thus \mathbf{F}_{PM} will change its direction when the PM crosses the loop plane ($z = 0$). In other words, the PM always receives a repulsive force from the superconducting loop during its entire moving process. (17) explains well the direction change of the force exerted on the PM, as reported in [3, 4].

In practice, a superconducting coil is composed of many turns, i.e. a series of current loops with distinct radius. Based on (14), the total current in a superconducting coil, I_{tot} , can be expressed as:

$$I_{tot} = \sum_{j=1}^N I_j = - \sum_{j=1}^N \frac{\mu_0 m}{2L_j} \frac{R_{cj}^2}{(R_{cj}^2 + z_{PM}^2)^{3/2}} \quad (18)$$

where N represents the number of turns in a superconducting coil, R_{cj} denotes the radius of the j -th turn, and I_j and L_j stand for the induced current and the equivalent inductance in the j -th turn, respectively. L_j can be approximated as L/N (L is the self-inductance of the entire coil), for simplification. Therefore, the average induced current in each turn of the superconducting coil can be written as:

$$I_{avg} = -\frac{1}{N} \sum_{j=1}^N \frac{\mu_0 m}{2L_j} \frac{R_{cj}^2}{(R_{cj}^2 + z_{PM}^2)^{3/2}}. \quad (19)$$

Accordingly, the repulsive force exerted on the PM can be calculated by:

$$\begin{aligned} F_{PM} &= \sum_{j=1}^N 2\pi R_{cj} I_j B_\rho \\ &= \sum_{j=1}^N 2\pi R_{cj} \cdot \frac{\mu_0 m}{2L_j} \frac{R_{cj}^2}{(R_{cj}^2 + z_{PM}^2)^{3/2}} \cdot \frac{3\mu_0 m}{4\pi} \frac{R_{cj} z_{PM}}{(R_{cj}^2 + z_{PM}^2)^{5/2}} \\ &= \sum_{j=1}^N \frac{3\mu_0^2 m^2}{4L_j} \frac{R_{cj}^4 z_{PM}}{(R_{cj}^2 + z_{PM}^2)^4}. \end{aligned} \quad (20)$$

It should be noted that, according to (14), the induced current in a superconducting loop appears to be independent of the intrinsic characteristics of the superconductor (e.g. the critical current), which intuitively seems unreasonable: in reality, an induced current beyond the critical current of a superconducting loop will not be expected, i.e. the induced current should be constrained by the current-carrying capacity

of the superconducting loop. In fact, to obtain (14), the perfect conductor approximation has been adopted for the superconducting loop, and thus the current carrying capacity of the superconducting loop has been assumed to be infinite. In other words, (14) should represent the upper limit of the current that can be induced in the superconducting loop for a fixed setup. In this paper, we exploit the perfect conductor approximation not only for enabling analytical calculation but more importantly we consider it reasonable to make such an assumption in the studied case: (a) as long as the induced current does not exceed the critical current of the HTS coil, the coil will stay superconducting with a very low resistance; (b) the electrical impedance of a superconducting coil is mainly determined by its inductance because its resistance is neglectable. To further illustrate the rationality of the perfect conductor approximation, relevant numerical modelling and experimental work will be presented as follows.

3. Modelling and measurement methods

In order to validate the proposed formulae, numerical modelling and experimental measurements were carried out at 77 K. The specifications of the adopted PM and Bi-2223 double pancake coil are shown in table 1.

3.1. Numerical modelling

Given that the entire system is both centrosymmetric and axisymmetric, the numerical model has been established with a 2D method based on the \mathbf{H} -formulation [9, 10] within COMSOL Multiphysics, as shown in figure 3.

On the basis of Faraday's law, Constitutive law, Ampere's law, and Ohm's law, the governing equation to be solved is obtained as [11–13]:

$$\nabla \times (\rho \nabla \times \mathbf{H}) = -\mu_0 \mu_r \frac{\partial \mathbf{H}}{\partial t} \quad (21)$$

where \mathbf{H} stands for the magnetic field, ρ denotes the electrical resistivity, μ_0 and μ_r represent the free space permeability and the relative permeability of the studied material, respectively.

The HTS double pancake coil has been modelled using the homogenization method proposed in [14, 15], with which the equivalent field dependence of the critical current of the HTS coil can be written as:

$$J_{c,eq}(B) = J_c(B) \cdot f_{HTS} = \frac{f_{HTS} J_{c0}}{\left(1 + \sqrt{k^2 B_z^2 + B_r^2 / B_0}\right)^\alpha} \quad (22)$$

where J_{c0} is the self-field critical current density of the HTS layer, B_z and B_r stand for the flux density components parallel and perpendicular to the wide surface of the HTS tape, respectively. $k = 0.061$, $\alpha = 0.76$, and $B_0 = 0.103$ T. f_{HTS} refers to the volume fraction of the HTS layer per unit cell (each cell is composed of an HTS tape and the surrounding insulation layer as well as the inevitable airgap). Therefore, considering f_{HTS} and the size parameters of the studied HTS double pancake coil, the equivalent self-field critical current density is taken as $J_{c0,eq} = f_{HTS} J_{c0} = 2 \times 10^8$ A m⁻².

Table 1. Specification of the studied PM and HTS coil.

Symbols	Quantity	Value
R_{PM}	Radius of the PM	12.5 mm
H	Height of the PM	20 mm
V	Volume of the PM	3125π mm ³
B_r	Remanent flux density of the PM	1.21 T
μ_0	Free space permeability	$4\pi \times 10^{-7}$ H m ⁻¹
W	Width of the Bi-2223 tape	4.2 mm
I_{c0}	Self-field critical current @ 77 K	110 A
R_i	Inner radius of the HTS coil	30.4 mm
R_o	Outer radius of the HTS coil	36.4 mm
N	Number of turns of the HTS coil	45
L	Self-inductance of the HTS coil	222.6 μ H

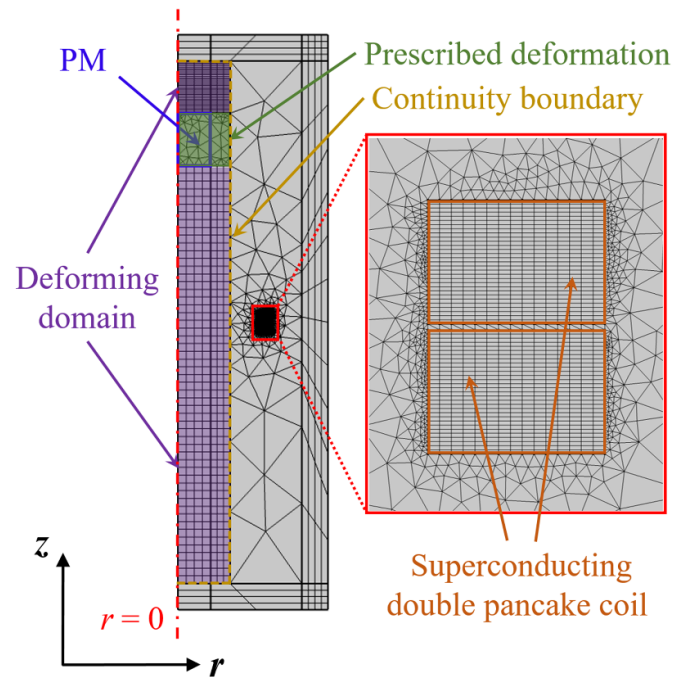


Figure 3. 2D numerical model of the energy conversion system characterised by a moving PM threading a homogenized superconducting double pancake coil.

In the numerical model, based on the above, three different electrical resistivities of the HTS will be adopted for comparison. When the HTS is approximated as a perfect conductor, we have:

$$\rho_{HTS} = 0. \quad (23)$$

With the Bean Model, the critical current density is constant, and thus from the E - J power law [16], we obtain:

$$\rho_{HTS} = \frac{E_0}{J_{c0,eq}} \cdot \left(\frac{J}{J_{c0,eq}}\right)^{n-1}. \quad (24)$$

Considering the $J_c(B)$ dependence [17], we get:

$$\rho_{HTS} = \frac{E_0}{J_{c0,eq}} \cdot \left(\frac{J}{J_{c0,eq}}\right)^{n-1}. \quad (25)$$

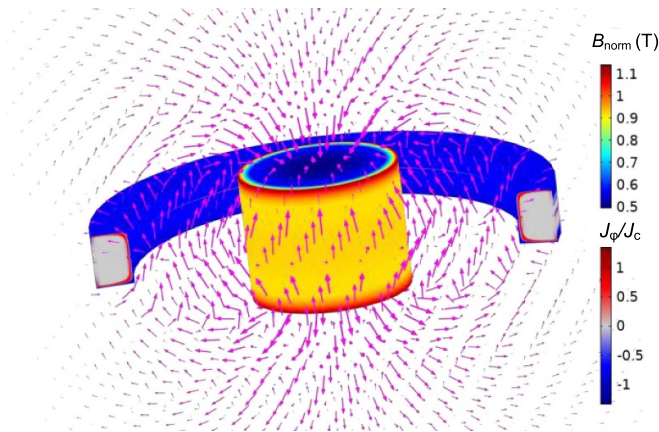


Figure 4. 3D view distribution of the current density load ratio (J_ϕ/J_c) inside the HTS coil and the spatial magnetic flux density (B_{norm}). The logarithmic arrows are used to depict the field direction. In this example, ρ_{HTS} has been featured by the equation (25).

In figure 3, except for the PM and HTS double pancake coil regions, all the other domains have been defined as air. The movement of the PM and its surrounding air is characterised by the moving mesh. The moving mesh of the PM and the air outside it (green region) is achieved by the prescribed deformation feature in COMSOL, and the moving air domains above and below the PM (purple areas) are set as deforming domain. The continuity boundary is located inside the air domain, which divides the moving mesh domain and the static mesh region [18]. An example 3D view of the current density load ratio (J_ϕ/J_c) distributions inside the HTS coil and the magnetic flux density (B_{norm}) distributions in the space (the field direction is represented by the logarithmic arrows) when the PM is situated at the coil plane ($z_{PM}=0$) is shown in figure 4.

3.2. Experimental measurement

The experimental procedures are the same as described in [3]. The experimental setup is shown in figure 5. A DS2-5N-type digital dynamometer with the precision of 10^{-3} N (manufactured by Dongguan City Intelligent Precision Instrument Co., Ltd) was utilized to detect the mechanical force exerted on the PM, between which an aluminum rod was exploited to rigidly connect the two parts. A FLUKE 319-type digital clamp meter was employed to acquire the induced current in the superconductor coil, with the resolution of 10^{-2} A. An N42 NdFeB magnet was adopted. The studied double pancake coil was wound from 45 turns of 4.2 mm wide Bi-2223 tapes, cooled by liquid nitrogen at 77 K inside an epoxy resin Dewar.

To avoid introducing excess inductance to the coil, the clamp meter was used to measure the current in a single turn.

4. Results and analyses

4.1. Macroscopic electromechanical performance

The current induced in each turn of the Bi-2223 double pancake coil and the mechanical force exerted on the PM obtained

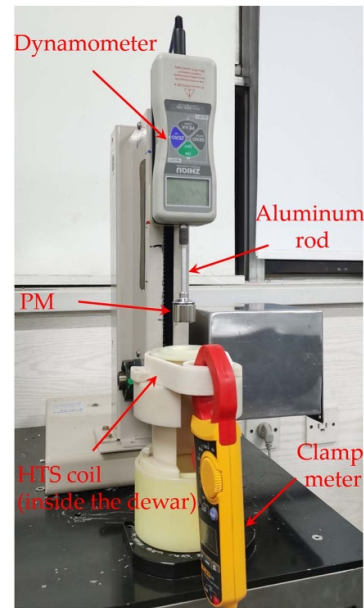


Figure 5. Experimental system for measuring the induced current in the HTS coil and the mechanical force exerted on the PM.

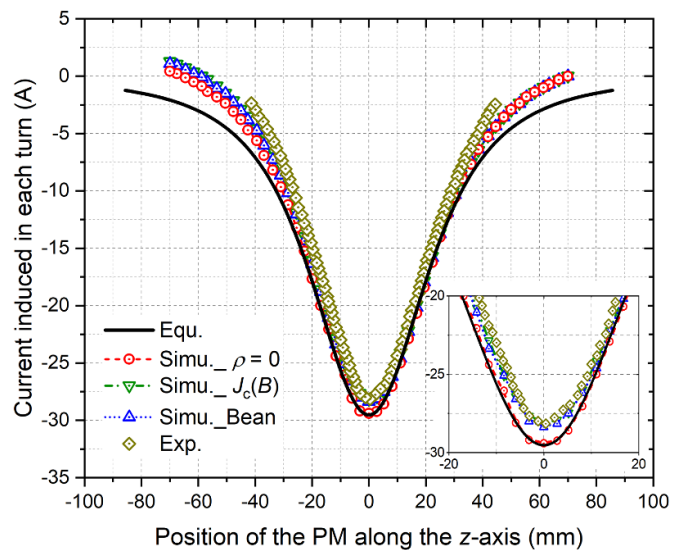


Figure 6. Current induced in each turn of the HTS double pancake coil. Equ represents the proposed equation (19), Simu refer to the simulation results in the three different cases, and exp denotes the experimental data.

by numerical modelling, experimental measurements, and the analytical formulae (19) and (20) have been depicted together in figures 6 and 7. The positive and negative values indicate the directions of the current and force in the coordinate system exhibited in figure 1.

It can be seen that in general the simulated results and measured data are in good accordance with the analytical equations proposed in this paper. The proposed equations comply well with the simulation of the perfect conductor cases with $\rho_{HTS} = 0$. Although the experimental data agree better with the simulation using the Bean model and the $J_c(B)$

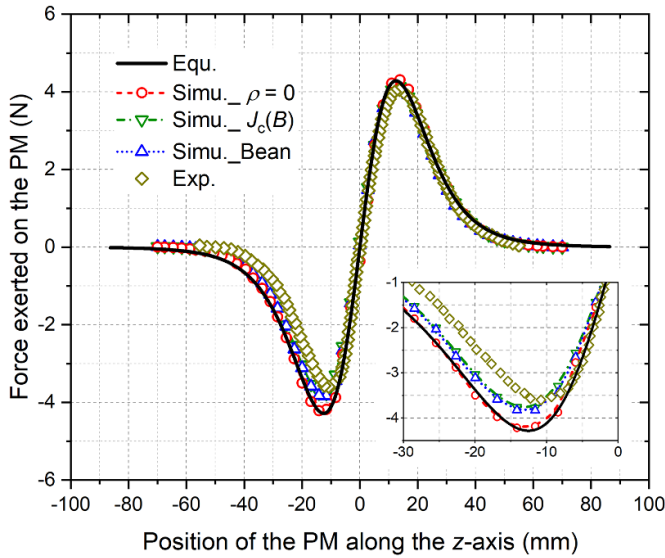


Figure 7. Mechanical force imparted on the PM by the HTS coil. Equ represents the proposed equation (20), Simu refer to the simulation results in the three different cases, and Exp denotes the experimental data.

dependence, the overestimated current calculated by the analytical equation gives a bias of approximately 1.3 A in terms of the peak current, which is acceptable compared to the experimental peak current 28.15 A with an error ratio of 4.61%. In the case of the peak mechanical force, the highest discrepancy between the analytical and experimental results is 0.25 N, which leads to an error ratio of 6.17%. Therefore, it can be concluded that the proposed equations can be conveniently exploited to estimate the current induced in the HTS coil and the mechanical force exerted on the PM with acceptable accuracy.

In terms of the peak values of the induced current and the mechanical force, it is not hard to understand that the results given by the proposed formulae and the simulation with $\rho_{\text{HTS}} = 0$ appear higher than the experimental data in that the superconductor has been approximated as a perfect conductor with ‘unlimited’ current-carrying capacity. The influence of the critical current of the HTS coil on the induced current and mechanical force will be discussed in detail in the following chapter. In addition, the two ends of the HTS coil were soldered with Sn–Bi alloy, which introduced a joint resistance in the range of 10^{-8} to 10^{-7} Ω . The induced current can be considered as a pulsed direct current (DC). Under the varying external magnetic field, a varying dynamic resistance can occur in the HTS coil [19–21]. The appearance of resistivity in the HTS coil can weaken the induced current, and thus the mechanical force.

It should also be noticed that the proposed formulae give rise to a much higher current at positions far from the coil plane, e.g. at $-80 \text{ mm} < z < -40 \text{ mm}$ and $40 \text{ mm} < z < 80 \text{ mm}$. In fact, to obtain (19) and (20), C in equation (13) has been taken as zero for the simplification of calculation under the assumption that the initial and ending positions ($\pm\infty$) of the PM is sufficiently far from the superconducting

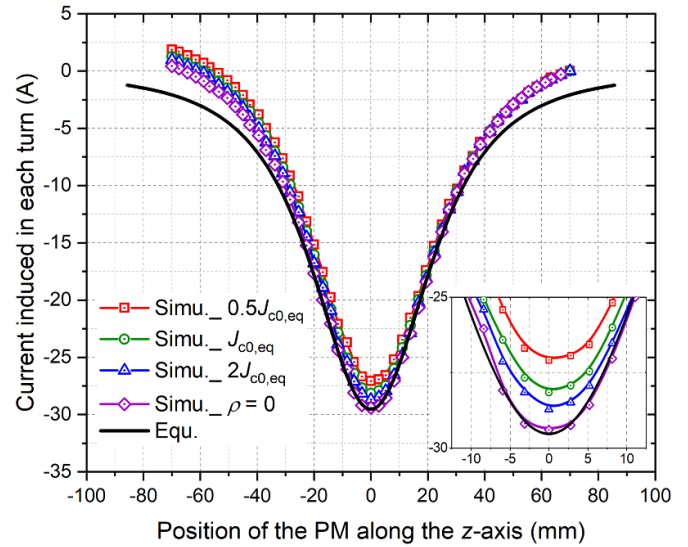


Figure 8. Influence of the self-field critical current on the current induced in each turn of the HTS double pancake coil. Equ represents the proposed equation (19), and Simu stands for the simulation results in the four different cases.

loop. However, in the experiment the PM moved between $z = \pm 60 \text{ mm}$, which indicates that the initial magnetic flux in the HTS coil was not zero, i.e. $C \neq 0$. As a result, in the experiment the induced current at the initial and ending positions of the PM was less than the analytical result, so is the force exerted on the PM.

4.2. Influence of the critical current

For further elucidation, in terms of the perfect conductor approximation adopted here, the influence of the critical current (density) of the HTS coil on the induced current and the force exerted on the PM will be studied through numerical modelling in this section. Without changing any sizes of any objects in the entire energy conversion system, three equivalent self-field critical current densities have been selected, which are $0.5J_{c0,eq}$, $J_{c0,eq}$, and $2J_{c0,eq}$, respectively.

The simulated induced currents in each turn and forces imparted on the PM at different self-field critical current densities have been separately depicted in figures 8 and 9. It can be found that the amplitude of the induced current is in a positive correlation with the critical current of the HTS coil, so is the mechanical force exerted on the PM. Therefore, it is confirmed that the induced current is no doubt constrained by the current-carrying capacity of the adopted conductors. In addition, the proposed analytical formulae, (19) and (20), represent the upper limit or the most ideal case for both the current and force.

From the perspective of macroscopic performance, the variation of the self-field critical current density does not bring significant changes to the induced current and mechanical force because of the superior current-carrying capacity of the HTS coil (given that the induced current is far less than the critical current of each Bi-2223 turn). However, from the microscopic view, the varying load ratio between the transport current

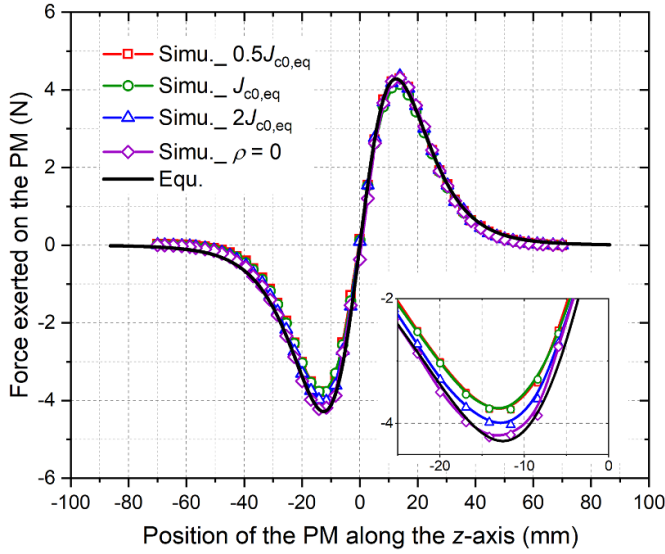


Figure 9. Influence of the self-field critical current on the mechanical force exerted on the HTS double pancake coil. Equ represents the formula (20), and Simu denotes the simulation results in the four different cases.

and the critical current can affect the distributions of currents and magnetic flux inside the HTS tapes, as shown in figure 10.

Figures 10(a)–(c) show the distributions of the magnetic flux density, B_{norm} , at $z = 0$, across the cross sections of three distinct HTS coils with the self-field critical current density equal to $0.5J_{c0,eq}$, $J_{c0,eq}$, and $2J_{c0,eq}$, respectively. Figures (d)–(f) demonstrate the B_r distributions at $z = 0$ of the three HTS coils with the self-field critical current density equal to $0.5J_{c0,eq}$, $J_{c0,eq}$, and $2J_{c0,eq}$, respectively. Figures (g)–(i) exhibit the distributions of the load ratios between the induced current density and the critical current density of the HTS coil, $J_\phi/J_{c,eq}$, with the self-field critical current density equal to $0.5J_{c0,eq}$, $J_{c0,eq}$, and $2J_{c0,eq}$, respectively.

It can be seen that, from (a)–(c), a higher magnetic field is allowed to penetrate to the inner side of the double pancake coil with increasing self-field critical current density, which implies that a higher current can be generated inside the HTS coil, agreeing well with figure 8. It should be pointed out that a higher external magnetic field can bring about a lower real critical current due to the $J_c(B)$ dependence, as shown in equation (22). However, the $J_c(B)$ dependence is mainly determined by the field component perpendicular to the wide surface of the HTS tape, B_r . Figures (d)–(f) present the B_r distributions in the three studied coil cross-sections. It can be seen that both ends of the innermost turns are more easily affected by the $J_c(B)$ dependence. Nevertheless, the perpendicular flux density is just on the order of dozens of mT, which is not sufficiently high to significantly drop the real critical current density. Taking the highest B_r , approximately 85 mT in (f) as an example, it can drive the critical current density drop from $2J_{c0,eq}$ to around $1.266J_{c0,eq}$, which is still higher than $J_{c0,eq}$. Therefore, under the $J_c(B)$ dependence, the induced current can still be carried by the HTS coils without a quench.

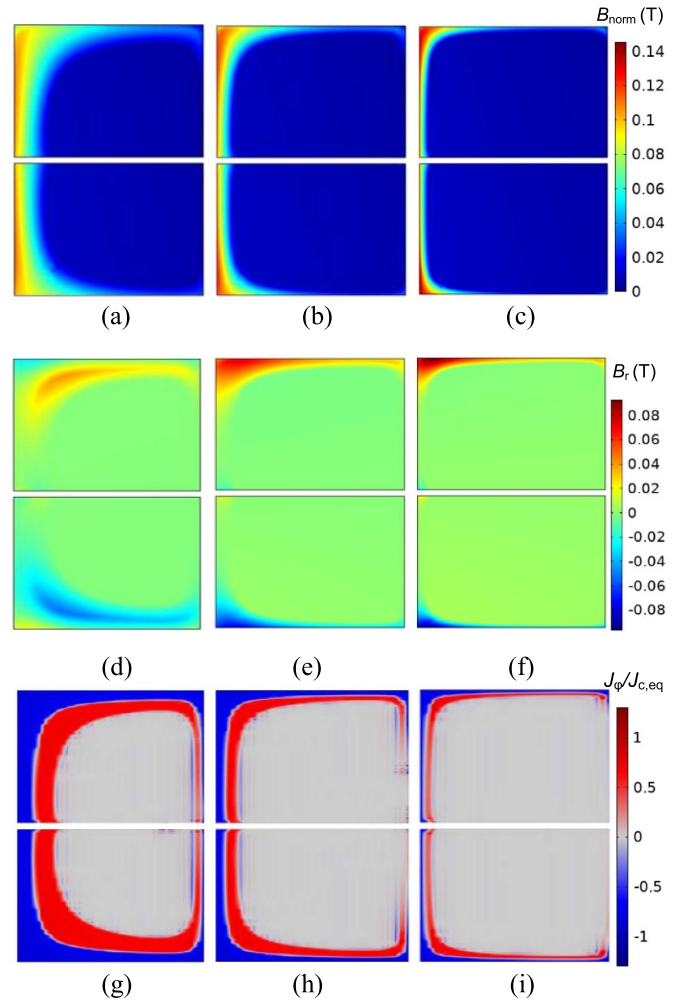


Figure 10. Current density and magnetic flux density distributions across the cross sections of three different HTS double pancake coils. Figures (a)–(c) refer to the B_{norm} distributions at $z = 0$, when the self-field critical current density is $0.5J_{c0,eq}$, $J_{c0,eq}$, and $2J_{c0,eq}$, respectively. Figures (d)–(f) represent the B_r distributions at $z = 0$, when the self-field critical current density is $0.5J_{c0,eq}$, $J_{c0,eq}$, and $2J_{c0,eq}$, respectively. Figures (g)–(i) exhibit the $J_\phi/J_{c,eq}$ distributions, at $z = -70$ mm, when the self-field critical current density is equal to $0.5J_{c0,eq}$, $J_{c0,eq}$, and $2J_{c0,eq}$, respectively.

From (g)–(i) it can be found that the distribution area of the induced current shrinks with the increase of the self-field critical current density. In fact, the induced currents in the three coils are all below their critical currents, and thus no quench happens during the entire dynamic process and the coils remain superconducting. Therefore, the induced currents in the three coils do not have a huge discrepancy because of their super current-carrying capacity, as shown in figure 8. As a result, inside the HTS coil with a lower self-field critical current, the induced current has to occupy more space to be carried.

4.3. Influence of the PM velocity

According to equations (14) and (17), the current induced in the superconducting loop and the mechanical force exerted

on the PM are determined by the position of the PM in the coordinate system, namely the distance between the PM and the coil centre. In other words, the velocity of the PM seems not relevant to the induced loop current and force experienced by the PM, which appears not easy to understand in that the changing rate of magnetic fields should directly determine the EMF in the coil and this field changing rate is closely related to the PM velocity. In order to clarify this issue, taking the absolute value of the PM velocity, v , as a constant, equations (19) and (20) can be rewritten as:

$$I_{\text{avg}} = -\frac{1}{N} \sum_{j=1}^N \frac{\mu_0 m}{2L_j} \frac{R_{c_j}^2}{\left[R_{c_j}^2 + (z_{\text{PM},0} \mp vt)^2 \right]^{3/2}} \quad (26)$$

$$F_{\text{PM}} = \sum_{j=1}^N \frac{3\mu_0^2 m^2}{4L_j} \frac{R_{c_j}^4 (z_{\text{PM},0} \mp vt)}{\left[R_{c_j}^2 + (z_{\text{PM},0} \mp vt)^2 \right]^4} \quad (27)$$

where $z_{\text{PM},0}$ denotes the initial position of the PM in the coordinate system ($z_{\text{PM},0} \neq 0$), and the \mp sign corresponds to the cases where the PM moves from $z_{\text{PM}} > 0$ to $z_{\text{PM}} < 0$ (v is towards the negative direction of the z -axis) and the PM moves from $z_{\text{PM}} < 0$ to $z_{\text{PM}} > 0$ (v is towards the positive direction of the z -axis), respectively. It is worth mentioning that though in this paper $z_{\text{PM}} = z_{\text{PM},0} - vt$, equations (14), (17), (19) and (20) are valid for both cases.

Taking the previously studied Bi-2223 double pancake coil as the research object, the induced currents in each turn and the forces imparted on the PM under different PM velocities obtained by the equations (26) and (27) as well as the \mathbf{H} -formulation based numerical model are presented together in figure 11.

It can be found that in general equations (26) and (27) agree well with the simulated results and a ‘pulse compression’ effect has appeared with increasing PM velocities: the current and force waveforms have been compressed in the time domain, and the compression ratio is proportional to the velocity changing rate. For example, when the PM velocity increases from 2.5 to 20 mm s⁻¹, the duration of the DC pulse has been reduced from 56 to 7 s, so is the force imparted on the PM. However, the fundamental waveform characteristics have not been changed and the amplitudes of the current and force remain the same despite the variation of PM velocities. In other words, if we combine the PM velocity and time node information to characterise the position of the PM, all the current and force waveforms in figure 11 will be converted back to figures 6 and 7, as correctly predicted by (19) and (20). Therefore, the current induced in the superconducting coil and the force exerted on the PM essentially depend on the position of the PM with respect to the coil.

In essence, the studied electromechanical interaction between a magnetic dipole and a superconducting loop is a result of the flux conservation property of the superconducting loop. As shown in equations (12) and (13), the dominant inductance of a superconducting circuit leads to a constant magnetic flux inside the loop. As a result, the induced current in the superconducting coil and the force exerted on the

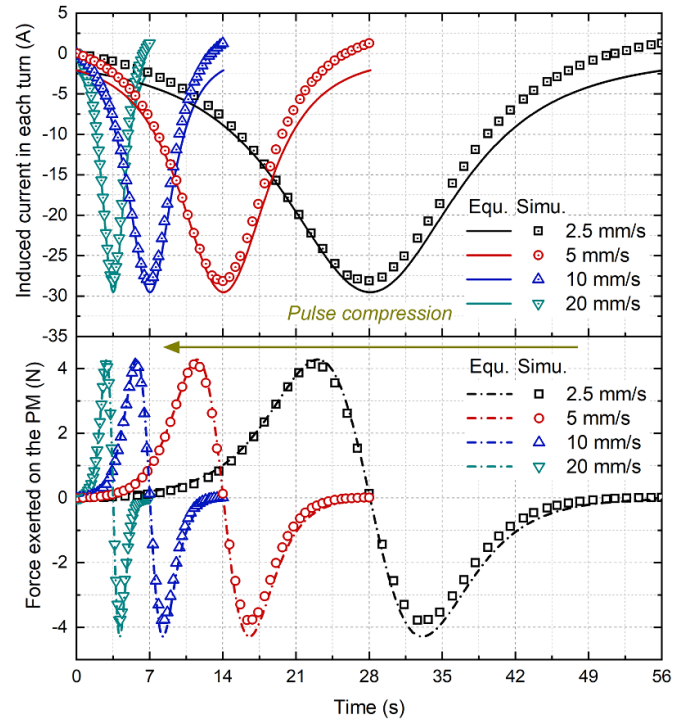


Figure 11. Variation of the current induced in each turn of the HTS double pancake coil and the force exerted on the PM in the time domain under various PM velocities. The results are obtained by equations (26) and (27) as well as the \mathbf{H} -formulation based numerical modelling, considering the $J_c(B)$ dependence.

PM are determined by the flux rather than the changing rate of the flux that accounts for the performance of a resistance-dominated normal conductive loop (more behaviour comparisons between a superconducting loop and a normal conductive one are presented in section 5). The magnetic flux brought to the superconducting loop by the moving PM is directly affected by the distance between them, and thus from the kinematic perspective, the interactions between a magnetic dipole and a superconducting loop are trajectory-dependent, as shown in (14) and (17). (14) and (17) also explain well the non-dependence of I and F_{PM} on the PM velocity demonstrated in figure 7 of [4].

4.4. Computational complexity

Compared with experimental measurements, numerical modelling is generally a more cost-effective and far less time-consuming method to estimate the electromechanical performance of the energy conversion system. The utilized computer is featured by the Intel Xeon CPU E3-1230 v6 @ 3.5 GHz and 16 GB RAM. Each of the \mathbf{H} -formulation based numerical models built in this paper is composed of 74 232 degrees of freedom, and it took no less than 11 h for every computation with a relative tolerance of 10^{-3} . As a comparison, the proposed formulae (19) and (20) can be easily programmed in MATLAB, which took only a few (around two) seconds to calculate the induced current and mechanical force. Therefore, the derived analytical equations can not only be used to account for the

anomalous interaction between a moving magnetic dipole and a closed superconducting loop but represent an efficient quantification tool to predict the macroscopic performance of the entire system with tolerable accuracy.

5. Discussion

In order to better comprehend the anomalous electromechanical effect happening to superconductors, we present here the behaviours of a normal conductive loop that is put in the same physical scene as the studied superconducting loop.

For a normal conductive circuit with the same radius R_c , different from (12), from Faraday's law, we have:

$$I = -\frac{1}{R} \frac{d\Phi}{dt} \quad (28)$$

where R is the resistance of the normal conductive loop. In (28), the term related to L has been neglected because its influence is far less than R . From (28) it can be seen that the induced current is determined by both the changing rate of magnetic flux over time and the resistance. Φ is displacement-dependent, thus $d\Phi/dt$ will be naturally velocity-dependent. The induced current I can therefore be derived as:

$$I = -\frac{1}{R} \frac{d\Phi}{dz_{PM}} \frac{dz_{PM}}{dt} = -\frac{3\mu_0 m}{2R} \frac{R_c^2 z_{PM}}{(R_c^2 + z_{PM}^2)^{5/2}} v \quad (29)$$

where v is the velocity (absolute value) of the moving PM. Equation (29) shows that the induced current in the normal conductive loop is z_{PM} -dependent, i.e. the direction of the current will change when the PM crosses the loop plane. Accordingly, the mechanical force exerted on the PM can be written as:

$$\begin{aligned} F_{PM} &= 2\pi R_c I B_\rho \\ &= 2\pi R_c \cdot \frac{3\mu_0 m}{2R} \frac{R_c^2 z_{PM}}{(R_c^2 + z_{PM}^2)^{5/2}} v \cdot \frac{3\mu_0 m}{4\pi} \frac{R_c z_{PM}}{(R_c^2 + z_{PM}^2)^{5/2}} \\ &= \frac{9\mu_0^2 m^2}{4R} \frac{R_c^4 z_{PM}^2}{(R_c^2 + z_{PM}^2)^5} v. \end{aligned} \quad (30)$$

It can be seen from (30) that the direction of the force exerted on the PM is not z_{PM} -dependent. The force is always along the positive direction of the z -axis, i.e. the PM firstly receives a repulsive force before crossing the loop plane, and then bears an attracting force after passing through the loop plane. Both (29) and (30) agree well with the conventional statement of Lenz's law.

Mathematically, the difference between a superconducting loop and a normal conductive one lies in the discrepancy between (14) and (28): equation (14) shows that the current induced in a superconducting loop is determined by the magnetic flux, but equation (28) demonstrates that the current in a normal conductive loop is decided by the changing rate of the magnetic flux. By its very nature, the nearly zero resistivity characteristic of superconductors (though carrying a pulsed DC) has caused the seeming 'Lenz's law-violated

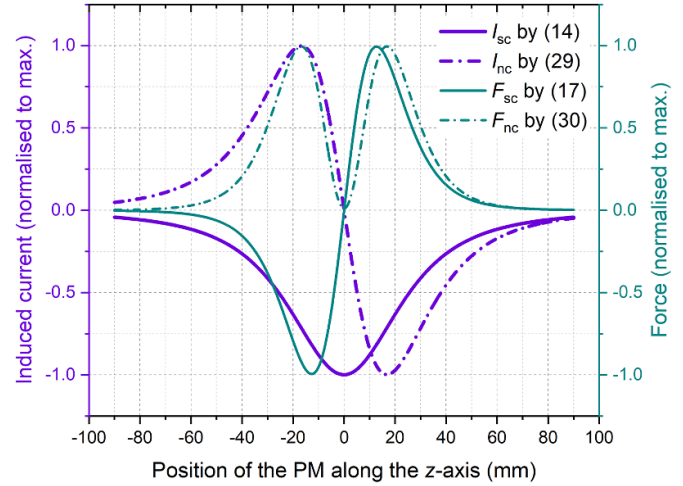


Figure 12. Normalised currents induced in a single superconducting loop and a single normal conductive circuit and forces exerted on the PMs in the two scenarios. All the currents and forces have been normalised to their maximum values. Initial parameters:

$R_c = 33.4$ mm, $R = 1$ Ω , $v = 1$ m s $^{-1}$, and the other parameters have been taken from table 1. sc: superconductor, nc: normal conductor.

effect', which leads to a quasi-persistent current and gives rise to constant magnetic flux inside the superconducting loop. In order to more intuitively exhibit the discrepancy between normal conductive and superconducting loops, the normalized induced currents and forces calculated based on (14), (17), (29), and (30) have been depicted together in figure 12.

From figure 12, it can be seen that the electromechanical behaviours of a superconducting loop are clearly different from a normal conductive one when the same PM threads them. In general, for a normal conductive loop, the induced current changes its circulating direction when the PM passes through the loop centre, just as what happens to the force exerted on the PM in the superconducting system. As a comparison, the induced current in a superconducting loop is featured by a DC pulse; however, the force imparted on the PM in the normal conductive system is characterised by two co-directional pulses. The performance of the normal conductive loop can be accurately estimated by Lenz's law, however, which is not the case for a superconducting one. Therefore, it is of great significance to derive equations (14) and (17) in this paper to qualitatively and quantitatively describe the anomalous electromechanical interactions between a magnetic dipole and a superconducting loop.

Let us revisit the seeming 'Lenz's law-violated phenomenon' from the perspective of energy conservation. Different from a resistance-dominant normal conductive coil, the zero resistivity of the superconducting loop gives rise to the energy conservation of the entire system (the air friction can be neglected). In other words, when the moving PM is approaching the superconducting loop, part of its kinetic energy will be converted to the electromagnetic energy stored in the loop and thus it should receive a repulsive force that does negative work. When the PM is leaving the superconducting loop, as the total magnetic flux inside the loop is decreasing and almost no

energy is dissipated in the superconductor, the stored electromagnetic energy will be given back to the PM. In this way, the PM will receive a repulsive force from the superconducting loop which does positive work.

From the perspective of energy conversion, it can also be concluded from figure 12 that the dominant resistance of a normal conductor governs the fact that the electromagnetic energy converted from the mechanical energy of the PM can not be effectively stored in the normal conductive loop because of instantaneous power dissipation. From this point, we can also propose here a ‘residual current’ concept because of the nearly zero resistance of the superconducting loop. When the PM moves from far to the loop centre, the electromagnetic energy will be stored in the superconducting loop in the form of an approximately persistent DC: since there exists no power dissipation, the DC is considered to circulate in the loop no matter how the PM moves afterward and thus it is named a ‘residual current’. Then, when the PM leaves the superconducting loop, according to Faraday’s law, an EMF in the opposite direction to the residual DC will be generated because of the reduction of the flux brought by the PM to the loop. The EMF will produce a current (named an ‘opposite current’) that circulates opposite to the circulating direction of the residual DC; consequently, the total current in the superconducting loop will decrease, as predicted by (14). The ‘residual current’ concept provides a way to understand the anomalous effect between a PM and a superconducting loop. However, we have to point out that: in order to drive the total current in the superconducting coil to decrease following the trend presented by figure 12 due to the moving away of the PM (z_{PM} varies from zero to negative), the generated ‘opposite current’ has to keep increasing, which is distinctively different from what happens to a PM moving away from a normal conductive loop: the induced current firstly increases and then decreases to zero. Therefore, the ‘residual current’ concept echoes well the anomalous electromechanical phenomenon that only happens to superconducting loops, and further confirms the rationality of the adopted perfect conductor approximation in theoretical analyses.

Regarding the formulae derivation, it needs to be clarified that, if both the electrical resistance and inductance of the superconducting coil are considered, we will get a highly non-linear equation combined with the non-linear $\mathbf{E}-\mathbf{J}$ power law, which appears not possible to obtain explicit formulae for the induced current and mechanical force. However, with the perfect conductor approximation, the proposed formulae in this paper are able to efficiently quantify the electromechanical performance of the entire energy conversion system with acceptable accuracy. Some researchers may stick to the point that superconductors are essentially different from perfect conductors on account of quantum effects such as the Meissner effect and quantization of magnetic flux. However, in our case, the quantum effects, e.g. the Meissner effect plays a minor role because the field generated by the PM easily goes beyond the lower critical field on the order of several mT and penetrates to the HTS tapes. Therefore, when studying the macroscopic performance of a superconducting system, the perfect conductor approximation remains a convenient tool to greatly ease calculations.

6. Conclusion

It has been recently discovered that when a PM passes through a superconducting loop, the current generated in the loop will keep the same circulating direction and thus the PM will always bear a repulsive force. The anomalous electromechanical effect seems to violate the extensively adopted fundamental statement of Lenz’s law applied to normal conductors and highlights the particular nature of superconductors. By its very nature, the anomalous electromechanical effect is mainly caused by the zero resistivity of the superconductor, which leads to constant magnetic flux inside the superconducting loop. As a result, the direction of the induced current turns invariant and the force exerted on the magnet becomes trajectory-dependent.

From the formulae derivation, it can be seen that Faraday’s law explains well the interactions between a magnetic dipole and a conductive loop, whether the loop is normal conducting or superconducting. However, the fundamental statement of Lenz’s law has to be reexamined in terms of ‘induced current’ and ‘mechanical force’ when it comes to superconductors. To put it more clearly, the description regarding the ‘induced current’ in the conductive loop or the ‘mechanical force’ imparted on the motion in the conventional statement should not be directly utilized to feature the electromechanical performance of such a system because the direct result of time-varying magnetic fields is an EMF that is directed to oppose the variation of magnetic fields. The generated current is just the macro characterization of the EMF and the intrinsic properties of the conductive loop, depending on whether the loop is resistance-dominant (for normal conductors) or inductance-dominant (for superconductors). Therefore, the current induced in a circuit due to a change in a magnetic field is directed to exert a mechanical force that opposes or favors the motion, depending on whether the circuit is superconducting.

This paper has revealed the physical mechanism behind the seeming ‘Lenz’s law-violated phenomenon’ in a closed superconducting loop with a rigorous analytical method and provided a significant supplement to Lenz’s Law applied to both normal conductors and superconductors. The studied device is essentially an energy conversion system, i.e. the mechanical energy of a moving PM and the electromagnetic energy of a superconducting magnet can achieve mutual conversion. Therefore, the anomalous electromechanical effect can spawn many applications related to energy storage/ conversion, e.g. regenerative braking in urban rail transit systems [7], electromagnetic ejection, and flux pumping, etc, which deserves more attention and research efforts in the future. The proposed formulae also provide an efficient and reliable analytical tool to quantify the interactions between magnetic sources and superconductors, which is far more cost-effective and time-saving than the FEM based numerical models and experiments.

Last but not the least, when studying the macroscopic performance of a superconducting system, the perfect conductor approximation for a superconductor can be a convenient tool to greatly ease analysis and calculations in many cases. There

should exist no reasons to simply neglect, abandon or even reject this method.






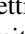
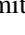

Data availability statement

All data that support the findings of this study are included within the article (and any supplementary files).

Acknowledgments

This work was supported by the 2021 IEEE Council on Superconductivity Graduate Study Fellowship in Applied Superconductivity. Hongye Zhang would like to give great thanks to Dr Mark Ainslie from the University of Cambridge for his helpful suggestions.

ORCID iDs

Hongye Zhang  <https://orcid.org/0000-0002-8960-4614>
 Tianhui Yang  <https://orcid.org/0000-0002-8481-0187>
 Wenxin Li  <https://orcid.org/0000-0003-4329-4136>
 Ying Xin  <https://orcid.org/0000-0001-7835-3832>
 Chao Li  <https://orcid.org/0000-0003-1058-4153>
 Matteo F Iacchetti  <https://orcid.org/0000-0001-6961-4789>
 Alexander C Smith  <https://orcid.org/0000-0001-6782-4627>
 Markus Mueller  <https://orcid.org/0000-0003-4859-3215>

References

- [1] Lenz E 1834 Ueber die Bestimmung der Richtung der durch elektodynamische Vertheilung erregten galvanischen Ströme *Annal. Phys. Chem.* **107** 483–94
- [2] Griffiths D 2013 *Introduction to Electrodynamics* 4th edn (Boston: Pearson) pp 315
- [3] Xin Y *et al* 2020 Superconductors and Lenz's law *Supercond. Sci. Technol.* **33** 055004
- [4] Li W *et al* 2021 Experimental study of electromagnetic interaction between a permanent magnet and an HTS coil *J. Supercond. Novel Magn.* **34** 2047–57
- [5] Hirsch J E 2007 Do superconductors violate Lenz's law? Body rotation under field cooling and theoretical implications *Phys. Lett. A* **366** 615–9
- [6] Li W *et al* 2021 Novel methods for measuring the inductance of superconducting coils and material resistivity *IEEE Trans. Instrum. Meas.* **70** 2001009
- [7] Li W *et al* 2021 Experimental study of a novel superconducting energy conversion/storage device *Energy Convers. Manage.* **243** 114350
- [8] Jackson J D 1998 *Classical Electrodynamics* 3rd edn (NY: Wiley)
- [9] Shen B, Grilli F and Coombs T 2020 Overview of H-formulation: a versatile tool for modeling electromagnetics in high-temperature superconductor applications *IEEE Access* **8** 100403–14
- [10] Pecher R *et al* 2003 3D-modelling of bulk type-II superconductors using unconstrained H-formulation *Proc. 6th Eur. Conf. Applied Superconductivity (Sorrento, Italy, September 2003)* pp 1–11
- [11] Zhang M and Coombs T 2012 3D modeling of high-Tc superconductors by finite element software *Supercond. Sci. Technol.* **25** 015009
- [12] Zhang H *et al* 2020 Dynamic loss and magnetization loss of HTS coated conductors, stacks, and coils for high-speed synchronous machines *Supercond. Sci. Technol.* **33** 084008
- [13] Grilli F *et al* 2013 Development of a three-dimensional finite-element model for high-temperature superconductors based on the H-formulation *Cryogenics* **53** 142–7
- [14] Zermeno V M R *et al* 2013 Calculation of alternating current losses in stacks and coils made of second generation high temperature superconducting tapes for large scale applications *J. Appl. Phys.* **114** 173901
- [15] Zermeno V M R and Grilli F 2014 3D modeling and simulation of 2G HTS stacks and coils *Supercond. Sci. Technol.* **27** 044025
- [16] Rhyner J 1993 Magnetic properties and AC-losses of superconductors with power law current-voltage characteristics *Physica C* **212** 292–300
- [17] Zhang H *et al* 2020 Modelling of electromagnetic loss in HTS coated conductors over a wide frequency band *Supercond. Sci. Technol.* **33** 025004
- [18] Li G *et al* 2021 Dynamic modelling methodology for an HTS energy converter using moving mesh *Supercond. Sci. Technol.* **34** 105006
- [19] Zhang H *et al* 2020 A full-range formulation for dynamic loss of HTS coated conductors *Supercond. Sci. Technol.* **33** 05LT01
- [20] Jiang Z *et al* 2017 Dynamic resistance of a high-Tc coated conductor wire in a perpendicular magnetic field at 77 K *Supercond. Sci. Technol.* **30** 03LT01
- [21] Zhang H *et al* 2020 Demarcation currents and corner field for dynamic resistance of HTS-coated conductors *IEEE Trans. Appl. Supercond.* (December 2020) **30** 1–5